https://doi.org/10.15407/ujpe68.4.284

V.B. NEIMASH,[1] P.E. SHEPELYAVYI,[2] A.S. NIKOLENKO,[2] V.V. STRELCHUK,[2] V.I. CHEGEL,[2] I.V. OLKHOVYK,[3] S.O. VORONOV[3]

[1] Institute of Physics, Nat. Acad. of Sci. of Ukraine
(46, Nauky Ave., Kyiv 03028, Ukraine)
[2] V.E. Lashkaryov Institute of Semiconductor Physics, Nat. Acad. of Sci. of Ukraine
(41, Nauky Ave., Kyiv 03028, Ukraine)
[3] National Technical University of Ukraine "Igor Sikorsky Kyiv Polytechnic Institute"
(37, Beresteiskyi Ave., Kyiv 03056, Ukraine)

THE ROLE OF TIN IN THE FORMATION OF MICRO- AND NANO-STRUCTURED SURFACES OF LAYERED Si–Sn–Si FILMS

The methods of Raman spectroscopy, scanning electron microscopy, atomic force microscopy, and X-ray fluorescence microanalysis are used to study the influence of tin on the shape and sizes of micro- and nano-structures arising on the surface of layered Si–Sn–Si films, as well as on the formation of Si nanocrystals in them during the tin-induced crystallization of amorphous silicon. In this work, the problems dealing with the experimental evaluation of the formation efficiency of Si nanocrystals in Si–Sn–Si films, the determination of the forms and scales of the film surface roughness, and the micro-distribution of impurities over the film surface and across the film thickness are tackled. The possibility of the formation of Si nanocrystals a few nanometers in size over most of the Si–Sn–Si film volume is experimentally confirmed. It is established for the first time that, during the production of such films using the thermal vacuum sputtering method, the thickness of a tin layer and its ratio to the thickness of silicon layers determine the shape and scale of the periodic surface relief structuring, which is important for the production of electronic devices. Quasi-spherical formations from 20 nm to 2–3 μm in diameter turned out to be the main element of the film surface relief structuring. The surface roughness induced by them can vary from a few nanometers to several tens of nanometers, depending on the layer deposition conditions. The shape of surface formations can change from cluster-like dendrites of the fractal type to convex ellipsoids and polygons. It is shown that the primary structuring occurs as the formation of a layer of hemispherical tin microdroplets already in the course of tin deposition. The secondary structuring occurs at the stage, when the second layer of silicon is deposited onto the layer of tin hemispheres. At this stage, a layer of the amorphous semiconductor is formed on the surface of the liquid metal, and this phenomenon is studied for the first time. The so-obtained amorphous silicon has a porous structure and consists of cluster-like dendrites of the fractal type about hundreds of nanometers in scale. The smallest dendrite elements also have a quasi-spherical shape 20–50 nm in diameter. Possible applications of the obtained results are discussed.

Keywords: amorphous silicon, tin, thin films, surface structure, nanocrystals, thermal vacuum sputtering.

1. Introduction

Silicon crystals a few nanometers in dimensions demonstrate light absorption properties according to the direct-band mechanism, which is typical of quantum dots, but they are two orders of magnitude more efficient than silicon single crystals. Furthermore, their band gap depends on the nanocrystallite size [1]. They are also resistant to the Stebler–Vronsky effect and suitable for their formation on flexible substrates. The application of nanosilicon for

Citation: Neimash V.B., Shepelyavyi P.E., Nikolenko A.S., Strelchuk V.V., Chegel V.I., Olkhovyk I.V., Voronov S.O. The role of tin in the formation of micro- and nano-structured surfaces of layered Si–Sn–Si films. *Ukr. J. Phys.* **68**, No. 4, 284 (2023). https://doi.org/10.15407/ujpe68.4.284.

Цитування: Неймаш В.Б., Шепелявий П.Є., Ніколенко А.С., Стрельчук В.В., Чегель В.І., Ольховик І.В., Воронов С.О. Роль олова у формуванні мікро- і наноструктури поверхні шаруватих плівок Si–Sn–Si. *Укр. фіз. журн.* **68**, № 4, 284 (2023).

the creation of cascade-type isomorphic heterostructures [2, 3] can essentially enhance the efficiency and reduce the cost of solar cells (SCs) due to the advantages of thin-film and roll technologies [4, 5].

One of the problems that hinder the practical implementation of the advantages of silicon nanocrystals is an insufficient development of technologies aimed at controlling the size and concentration of Si nanocrystals at economically justified formation rates. Therefore, in spite of a large number of already available nc-Si fabrication technologies, much attention is paid to their improvement and the search for new ones (see, e.g., works [6–12]).

One of the promising ways in this direction is the application of the phenomenon of the metal-induced crystallization (MIC) of amorphous silicon [13–17]. During the last decade, the possibility of the formation of 2–5-nm Si nanocrystals in an amorphous Si matrix was experimentally demonstrated with the help of the low-temperature tin-induced crystallization of amorphous Si [18–20]. Those nanocrystals occupy up to 80% of the matrix volume. The obtained experimental results are interpreted by engaging the MIC mechanism, which was proposed in works [20,21] and theoretically substantiated in work [22].

The MIC mechanism differs substantially from those known for other metals [13,15–17]. More specifically, silicon nanocrystals are formed as a result of a cyclic repetition of the formation and decay of a supersaturated solution of silicon in tin in a narrow moving eutectic layer arising at the interface between amorphous silicon and metallic tin. It turned out that, as a result, an amorphous-crystalline composite can be formed in layered Si–Sn–Si films, with up to 90% of the composite volume being occupied by silicon nanocrystals a few nanometers in size [23]. Since tin is isovalent to silicon, its atoms are electrically neutral in Si and, in contrast to most other metals, do not affect the electrical and recombination parameters of the semiconductor. This circumstance comprises a principal advantage of applying just tin for MIC.

However, a considerable surface and bulk nonuniformity of such films is a substantial obstacle to the practical application of the tin-induced crystallization of amorphous silicon in the production of nanosilicon films for solar cells. This remark concerns both amorphous films of silicon-tin alloys [20] and layered Si–Sn–Si films [24]. Those factors significantly hamper the application of the films of this type in the standard planar technology of silicon-based device manufacture. Therefore, the origins of their appearance and the relevant mechanisms have to be studied. On the other hand, the same factors make it possible to create principally new types of micro- and nano-structuring of the surface of silicon films, whose properties and application prospects have not been practically studied yet. Therefore, the aim of this work, as a continuation of work [24], was to experimentally study and analyze the role of tin in the structuring of just the surface relief of Si–Sn–Si films.

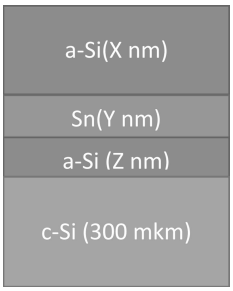

Fig. 1. Schematic diagram illustrating the arrangement and designation of silicon and tin layers in the researched structures

2. Experimental Part

As research objects, three-layer film structures "amorphous silicon–metallic tin–amorphous silicon" on substrates made of single-crystalline KEF-4.5 silicon were taken. They were fabricated by successively depositing the vapor of silicon (99.999%), tin (99.92%), and again silicon, which were thermally evaporated in the vacuum from electrically heated tantalum vaporizers. Deposition was performed onto 300-μm substrates made of single-crystalline silicon with the electron purity grade, which had been polished to the 6th degree of perfection, at a substrate temperature of about 150 °C. The deposition sequence was as follows (see Fig. 1): a layer of amorphous silicon (Z) onto the single-crystal substrate, a layer of tin (Y) onto the top of layer Z, and the second layer of amorphous silicon (X) onto the top of layer Y.

The thicknesses of layers X, Y, and Z were discretely varied within an interval of 5–200 nm with an increment of 5–50 nm, and they were estimated from the frequency change of a quartz resonator, the surface of which was subjected to the parallel deposition. All deposition procedures were carried out in the same vacuum chamber without depressurization,

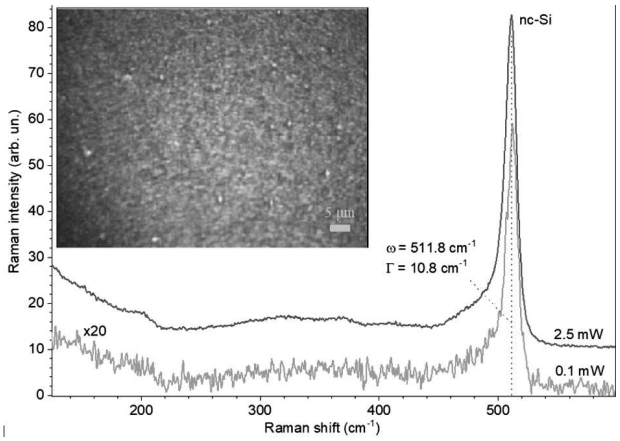

Fig. 2. Raman spectra of the surface layer of the a-Si(∼50 nm)\Sn(∼100 nm)\a-Si(∼200 nm) film after its heat treatment at 800 °C. The spectra were registered at two different powers of a laser excitation beam. The optical microscopy image of the surface of the studied a-Si(∼50 nm)\ Sn(∼100 nm)\a-Si(∼200 nm) structure is shown in the inset

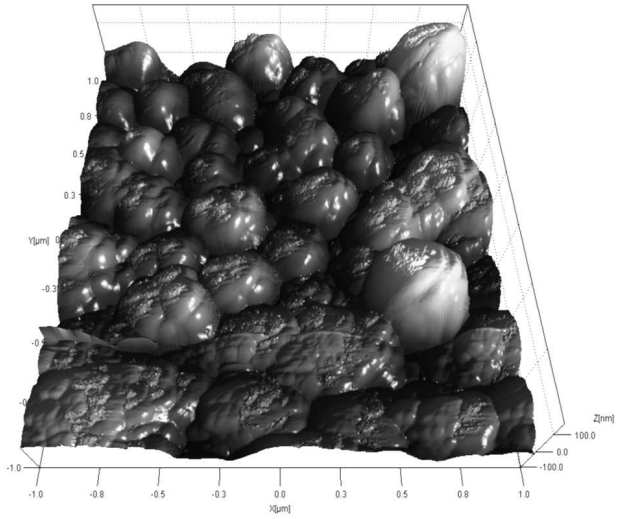

Fig. 3. AFM image of the surface of the studied a-Si(∼50 nm)\Sn(∼100 nm)\a-Si(∼200 nm) structure

at a residual pressure of 10^{-3} Pa, and making sequential use of three different evaporators. The amorphous silicon layer Z (closest to the substrate) was required for the better adhesion of tin layer Y to the single-crystalline silicon substrate. During the further heat treatments, the tin layer Y provided conditions for the transition of silicon from the amorphous state into the single-crystalline one owing to the MIC effect [22]. The consequences of this transition in the silicon layer X were studied using the Raman spectroscopy methods on a Horiba Jobin Yvon T64000 spectrometer equipped with an Olympus BX41 confocal microscope and a thermoelectrically cooled CCD detector.

Main attention in this work was focused on the qualitative and quantitative characterization of the relief of the surface layer in the experimental structures, as well as on the spatial distribution of the elemental composition over the surface and across the thickness of the Si–Sn–Si structures with various ratios between the thicknesses of the silicon and tin layers. For this purpose, secondary-electron scanning electron microscopes (SEMs) with X-ray microprobes JEM-2000 FXII, a scanning VEGA 3 SBU microscope, and a NanoScope IIIa Dimension 3000 atomic force microscope (AFM) were used. Detectors of two types were applied in the SEM research: a BSE detector of scattered electrons, which was arranged at an angle of about 60° with respect to the electron beam direction, and a ring InBeam detector, which encircled the scanning beam and mainly registered electrons reflected at small angles with respect to it.

3. Results and Discussion

As an example, Fig. 2 demonstrates a characteristic Raman spectrum of the outer layer X in the structure a-Si(∼50 nm)

Sn(∼100 nm) a-Si(∼200 nm) that was heat-treated in the vacuum at 800 °C. One can see that if the laser power at the specimen equals 0.1 mW, a signal from the nanocrystalline silicon (nc-Si) phase is registered at a frequency of 511.8 cm^{-1} (the half-width of the band is about 10.8 cm^{-1}), which corresponds to a size of nanocrystals of about 3 nm and their volume fraction of about 90%. The growth of the power to 2.5 mW leads to an insignificant low-frequency shift of the nc-Si peak to 511.0 cm^{-1} (the band half-width is about 10.9 cm^{-1}) as a result of the laser-induced heating. The laser beam leaves no traces on the surface, which means that the laser heating of the specimen does not elevate the temperature above the tin melting point, or that there is no tin in the free state.

The inset in Fig. 2 exhibits an optical microscopy image of the surface of the examined structure. An inhomogeneous image character testifies to a substantial surface roughness. This conclusion is confirmed by the results of AFM studies (Figs. 3 to 6) carried out on similar a-Si (∼50 nm) Sn (∼100 nm)\ a-Si (∼200 nm) specimens. They testify that the surface

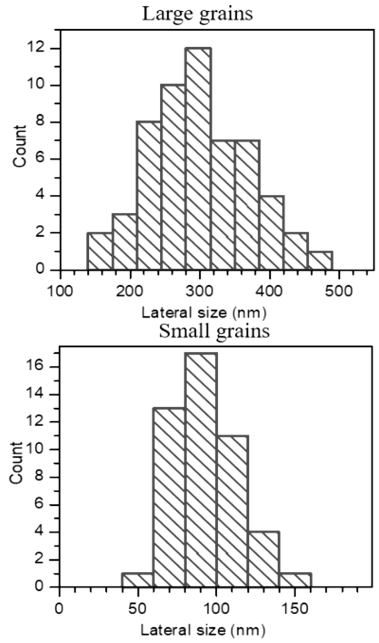

Fig. 4. Histograms of the lateral sizes of the quasi-spherical grains in the surface relief of Si\Sn\Si structures

of the specimens has a granular structure. The grains' shape can be characterized as quasi-spherical.

Smaller grains can be clearly distinguished on the surface of large grains (clusters). As it follows from the grain size distribution shown in Fig. 4, the average lateral size of large grains equals about 300 nm, and that of small grains is about 100 nm.

In Fig. 5, a histogram of the heights of quasi-spherical grains (the relative distribution of the difference between the grain's top and the valley) composing the surface relief. But the roughness of the researched structures at the quantitative level is most clearly illustrated by the profile of the specimen surface relief depicted in Fig. 6. It should be noted that, in this figure, as well as in Fig. 4, the scale along the abscissa axis is indicated in the micrometer units, and the scale along the ordinate axis in the nanometer ones.

This circumstance has to be taken into account when visually comparing the graphic representation of the results obtained using the atomic force microscopy and electron microscopy methods (see Figs. 7 to 9, where the dimensions along both axes are shown on the same scale). In particular, Fig. 7 illustrates SEM images of the surface of Si–Sn–Si struc-

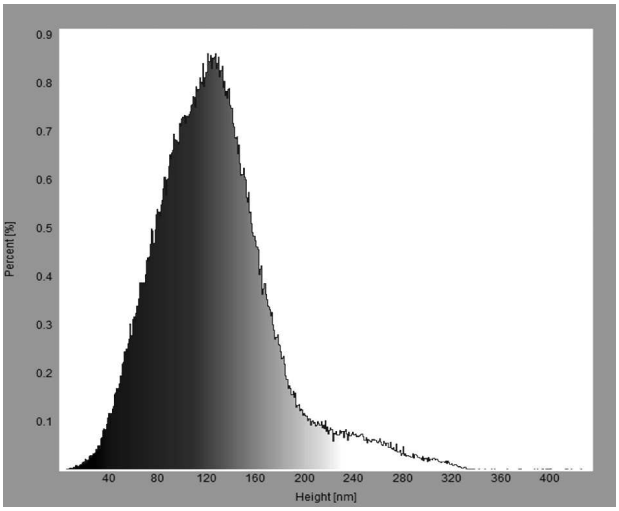

Fig. 5. Histogram of the heights of the quasi-spherical grains in the surface relief of Si\Sn\Si structures obtained on the basis of AFM studies

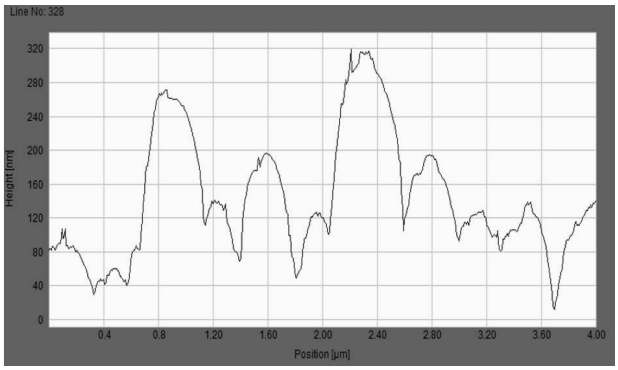

Fig. 6. Profile of the specimen surface relief obtained on the basis of AFM studies

tures with various thicknesses of the tin layer Y. From this figure, one can see that if the thickness of the tin layer decreases from 100 to 25 nm, the shape of the a-Si surface structuring changes from elliptical (for the layer thickness ratio a-Si\Sn\Si = 50\100\200 nm) to spherical (for a-Si\Sn\Si = 50\50\200 nm) and, further, to convex irregular 4-, 5-, and 6-hedra (for a-Si\Sn\Si = 50\25\200 nm). The corresponding lateral size of the surface formations decreases from 1000 to 200 nm, and the surface relief structuring becomes more pronounced.

Figure 8 presents a SEM image of a cleaved end of a three-layer structure with the layer thickness ratio Si\Sn\Si = 50\25\200 nm. Four zones with differ-

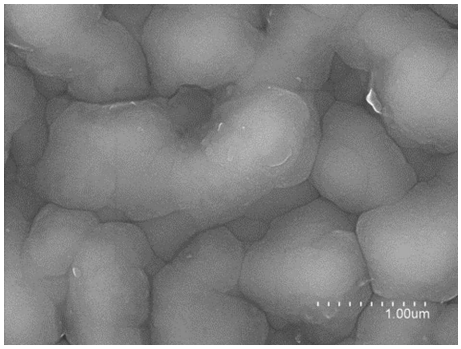

a

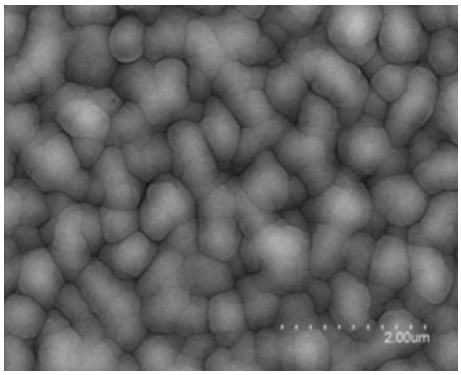

b

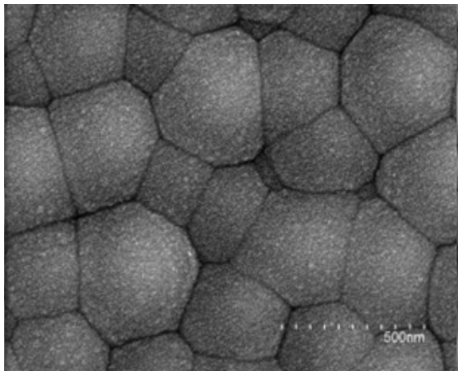

c

Fig. 7. SEM images of the surfaces of Si\Sn\Si layered structures with various thicknesses of the Sn layer

ent contrast levels are observed. The first zone from the bottom is uniformly dark and corresponds to the single-crystalline silicon substrate. A thin light gap separates it from the second dark zone corresponding to the bottom layer of amorphous silicon. Above it, one can see a layer of hemispheres corresponding to tin droplets, and the silicon layer is located even higher.

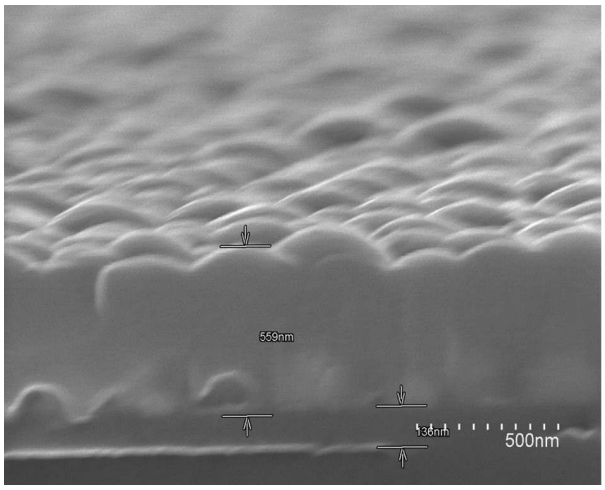

Fig. 8. SEM image of the cross-section of a three-layer structure Si\Sn\Si = 50\25\200 nm

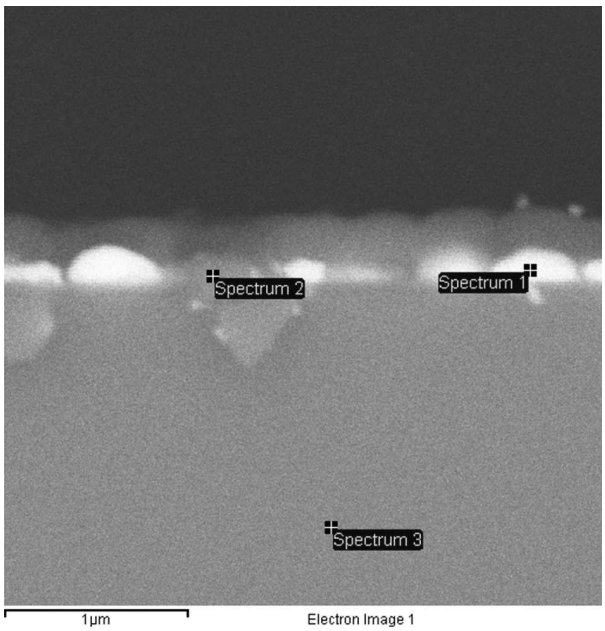

Fig. 9. SEM image of the end face of the Si–Sn–Si layered structure. The sites where the local elemental composition in the formed film was analyzed using X-ray fluorescence spectroscopy are marked. The results of this analysis are quoted in Table

In Fig. 9, a SEM image of the end face of a layered Si\Sn\Si structure is exhibited. In addition, the places are marked, where the elemental composition was analyzed with the help of the X-ray fluorescence analysis.

When considering the data in Table, it should be taken into account that if the method of X-ray fluorescence microanalysis is applied to silicon, the geometric size of the fluorescence excitation zone is about a micrometer and substantially exceeds the diameter of the exciting electron beam. Therefore, if objects of the same or smaller size are considered, it is necessary to account for the fact that the evaluation of the elemental content gives a value averaged over the excitation zone. In the case of film cross-section (i.e., when the excitation beam falls on the film's end), this zone can substantially exceed the size of the researched micro-object. Accordingly, the result of such an analysis reflects the elemental content in a volume that is larger than the volume of the micro-object. That is why the tin content in spectrum 1 equals only 35% rather than 100% expected on the basis of the image contrast. A high, at a level of 23–30%, carbon content in the examined spectra is a result of the residual contamination of the microscope chamber made during earlier experiments with carbon composites. This conclusion is evidenced by the equality of the carbon contents in the spectra of single-crystalline substrate and deposited layers.

Note that the roughness of the formed film is also visible in the SEM image of the specimen surface (see Fig. 9). A more detailed image of the latter obtained in the InBeam mode with the application of a ring detector arranged round the scanning beam (this detector mainly registered electrons reflected at small angles) is shown in Fig. 10. The operation in the InBeam mode made it possible to notice that the quasi-spherical formations on the surface of our specimens had a more complicated structure. A higher magnification showed that they are composed of smaller quasi-spherical formations with a size of one order of magnitude smaller. The smallest formations that can be clearly distinguished here had a size less than 20 nm. They formed structures similar to three-dimensional dendrites of the fractal type.

Table 1. **Elemental compositions of the formed films according to the results of X-ray fluorescence spectroscopy**

Spectrum	All results in weight					
	In stats	C	O	Si	Sn	Total
Spectrum 1	Yes	22.95	6.96	34.67	35.42	100
Spectrum 2	”	29.72	5.00	55.19	10.09	100
Spectrum 3	”	29.59	0.00	70.41	0.00	100

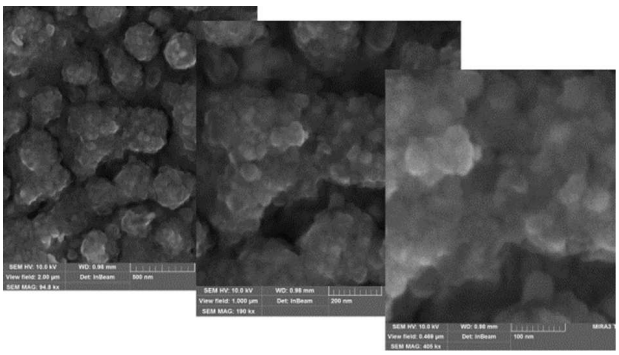

Fig. 10. SEM images of the outer surfaces of layer X of specimen 3 obtained at various magnifications

The obtained results are in good agreement with the AFM data on the film surface roughness and granularity, which are shown in Figs. 3 to 6. Actually, the formed films are porous silicon with pore diameters ranging from 20 to 200 nm. The surface tension forces and weak adhesion of tin to silicon bring about the formation of tin droplets (hemispheres) on the surface of silicon layer during its deposition onto the lower side of the heated substrate. For the same reasons, the further deposition of silicon onto the wavy surface of liquid tin gives rise, at a certain stage, to the formation of an island film of amorphous silicon on this surface and the extrusion (outflow) of new, smaller hemispheres (droplets) of liquid tin. If the Si deposition continues, those processes can also continue with the formation of smaller and smaller structures of the same type. This circumstance can explain the fractal character of the surface structuring in the researched specimens.

4. Conclusions

1. The possibility of obtaining an amorphous-crystalline nanocomposite via the tin-induced crystallization of amorphous silicon in layered Si–Sn–Si films has been experimentally demonstrated. The composite contained silicon nanocrystallites with an average size of 3 nm. The fraction of nanocrystallites in the film volume exceeded 90%.

2. The surface of the layered Si–Sn–Si films fabricated using the thermal vacuum deposition method has a structured relief in the form of quasi-spherical formations with a lateral size varying from 20 nm to 2–3 μm. Depending on the tin layer thickness, their

shape (together with the size) varies: from convex ellipsoids and polygons to cluster-like dendrites of the fractal type. Such dendrites could create a porous layer (the pore sizes ranged from 1 to 100 nm) of amorphous silicon, the physical properties of which have not been studied yet.

3. The primary origin of the surface structuring in Si–Sn–Si films is the melting of the tin layer and its decay into micro-droplets in the course of tin and silicon deposition. The formation of Sn micro-droplets stimulated by the action of surface tension forces under the conditions of weak wetting of silicon with tin is a factor responsible for the quasi-spherical relief of the liquid tin layer. The further deposition of silicon atoms onto this layer gives rise to the formation of the outer surface of the structure.

4. The obtained results can be used to reduce or increase the surface roughness of Si–Sn–Si films, which is important for the development of available technologies aimed at the formation of nanosilicon films for the ghtrhdevice construction and the creation of coatings capable of effective light scattering. Furthermore, they open certain prospects for the development of new methods for the manufacture of porous silicon via the thermal vacuum deposition method.

5. The results obtained in this work can be used to improve the available technologies used for the formation of nanosilicon films for solar cells, as well as for the production of silicon-isomorphic light-scattering coatings.

This work was sponsored in the framework of the Target complex programme of the National Academy of Sciences of Ukraine "Fundamental problems of creating new nanomaterials and nanotechnologies" (project No. 12\20-H "Tin-induced bulk nanocrystallization and surface nanostructuring of thin amorphous silicon films".

1. M.C. Beard, J.M. Luther, A.J. Nozik. The promise and challenge of nanostructured solar cells. *Nat.Nano* **9**, 951 (2014).
2. Z.I. Alferov, V.M. Andreev, V.D. Rumyantsev. Solar photovoltaics: Trends and prospects. *Semiconductors* **38**, 899 (2004).
3. B. Yan, G. Yue, X. Xu, J. Yang, S. Guha. High efficiency amorphous and nanocryistallinesillicon solar cells. *Phys. Status Solidi (a)* **207**, 671 (2010).
4. N.S. Lewis. Toward cost-effective solar energy use. *Science* **315**, 798 (2007).
5. R. Søndergaard, M. Hösel, D. Angmo, T.T. Larsen-Olsen, F.C. Krebs. Roll-to-roll fabrication of polymer solar cells. *Mater. Today* **15**, 36 (2012).
6. M. Birkholz, B. Selle, E. Conrad, K. Lips, W. Fuhs. Evolution of structure in thin microcrystalline silicon films grown by electron-cyclotron resonance chemical vapor deposition. *J. Appl. Phys.* **88**, 4376 (2000).
7. B. Rech, T. Roschek, J. Müller, S. Wieder, H. Wagner. Amorphous and microcrystalline silicon solar cells prepared at high deposition rates using RF (13.56 MHz) plasma excitation frequencies. *Sol. Energ. Mater. Sol. Cells* **66**, 267 (2001).
8. M.K. vanVeen, C.H.M. van der Werf, R.E.I. Schropp. Tandem solar cells deposited using hot-wire chemical vapor deposition. *J. Non. Cryst. Solids* **338–340**, 655 (2004).
9. Y. Mai, S. Klein, R. Carius, H. Stiebig, L. Houben, X. Geng, F. Finger. Improvement of open circuit voltage in microcrystalline silicon solar cells using hot wire buffer layers. *J. Non. Cryst. Solids* **352**, 1859 (2006).
10. H. Li, R.H. Franken, R.L. Stolk, C.H.M. van der Werf, J.K. Rath, R.E.I. Schropp. Controlling the quality of nanocrystalline silicon made by hot-wire chemical vapor deposition by using a reverse H2 profiling technique. *J. Non. Cryst. Solids* **354**, 2087 (2008).
11. R. Amrani, F. Pichot, L. Chahed, Y. Cuminal. Amorphous-nanocrystalline transition in silicon thin films obtained by argon diluted silane PECVD. *Cryst. Struct. Theor. Appl.* **1**, 57 (2012).
12. G. Fugallo, A. Mattoni. Thermally induced recrystallization of textured hydrogenated nanocrystalline silicon. *Phys. Rev. B* **89**, 045301 (2014).
13. O. Nastand, A.J. Hartmann. Influence of interface and Al structure on layer exchange during aluminum-induced crystallization of amorphous silicon. *J. Appl. Phys.* **88**, 716 (2000).
14. M. Jeon, C. Jeong, K. Kamisako, Tin induced crystallisation of hydrogenated amorphous silicon thin films. *Mater. Sci. Technol.* **26**, 875 (2010).
15. M.A. Mohiddon, M.G. Krishna. Growth and optical properties of Sn–Si nanocomposite thin films. *J. Mater. Sci.* **47**, 6972 (2012).
16. D. Van Gestel, I. Gordon, J. Poortmans. Aluminum-induced crystallization for thin-film polycrystalline silicon solar cells: Achievements and perspective. *Sol. Energ. Mater. Sol. Cells* **119**, 261 (2013).
17. M.A. Mohiddon, M.G. Krishna. Metal induced crystallization. In: *Crystallization – Science and Technology.* Edited by A. Marcello (InTech, 2012), p. 461.
18. V.V. Voitovych, V.B. Neimash, N.N. Krasko, A.G. Kolosiuk, V.Y. Povarchuk, R.M. Rudenko, V.A. Makara, R.V. Petrunya, V.O. Juhimchuk, V.V. Strelchuk. The effect of Sn impurity on the optical and structural properties of thinsilicon films. *Semiconductors* **45**, 1281 (2011).
19. V.B. Neimash, V.M. Poroshin, A.M. Kabaldin, V.O. Yukhymchuk, P.E. Shepelyavyi, V.A. Makara, S.Y. Larkin.

Microctructure of thin Si–Sn composite films. *Ukr. J. Phys.* **58**, 865 (2013).
20. V. Neimash, V. Poroshin, P. Shepeliavyi, V. Yukhymchuk, V. Melnyk, A. Kuzmich, V. Makara, A.O. Goushcha. Tin induced a-Si crystallization in thin films of Si–Sn alloys. *J. Appl. Phys.* **114**, 213104 (2013).
21. V.B. Neimash, A.O. Goushcha, P.E. Shepeliavyi, V.O. Yukhymchuk, V.A. Dan'ko, V. Melnyk, A. Kuzmich. Mechanism of tin-induced cristallization in amorphous silicon. *Ukr. J. Phys.* **59**, 1168 (2014).
22. V.B. Neimash, A.O. Goushcha, P.Y. Shepeliavyi, V.O. Yuhymchuk, V.V. Melnyk, A.G. Kuzmich. Self sustained cyclic tin induced crystallization of amorphous silicon. *J. Mater. Res.* **30**, 3116 (2015).
23. V.B. Neimash, A.S. Nikolenko, V.V. Strelchuk, P.Ye. Shepelyavyi, P.M. Litvinchuk, V.V. Melnyk, I.V. Olkhovyk. Influence of laser light on the formation and properties of silicon nanocrystals in a-Si/Sn layered structures. *Ukr. J. Phys.* **64**, 522 (2013).
24. V.B. Neimash, P.Ye. Shepelyavyi, A.S. Nikolenko, V.V. Strelchuk, V.I. Chegel. Micro- and nanostructure of layered Si\Sn\Si films, formed by vapor deposition. *J. Nanomater.* **2022**, 7910708 (2022).

Received 14.12.22.
Translated from Ukrainian by O.I. Voitenko

В.Б. Неймаш, П.Є. Шепелявий,
А.С. Ніколенко, В.В. Стрельчук,
В.І. Чегель, І.В. Ольховик, С.О. Воронов

РОЛЬ ОЛОВА У ФОРМУВАННІ МІКРО- І НАНОСТРУКТУРИ ПОВЕРХНІ ШАРУВАТИХ ПЛІВОК Si–Sn–Si

Методи Раманівської спектроскопії, растрової електронної мікроскопії, атомно-силової мікроскопії і рентґено-флуоресцентного мікроаналізу застосовані з метою дослідження впливу олова на форму і розміри мікро- та наноструктури поверхні шаруватих плівок Si–Sn–Si, а також на утворення в них нанокристалів Si під час індукованої оловом кристалізації аморфного кремнію. В даній роботі вирішувалися задачі експериментальної оцінки ефективності формування нанокристалів Si в плівках Si–Sn–Si, а також визначення форм і масштабів шорсткості поверхні плівок, мікророзподілу домішок по їх площі і перерізу. Експериментально підтверджено можливість формування нанокристалів Si масштабу одиниць нанометрів в більшій частині об'єму плівок Si–Sn–Si. Вперше встановлено, що при виготовленні таких плівок методом термічного вакуумного напилення товщина шару олова та її співвідношення з шарами кремнію визначають форму і масштаб періодичної структуризації рельєфу поверхні, яка важлива для виготовлення реальних електронних приладів. Головним елементом структурування рельєфу поверхні плівок виявилися квазисферичні утворення діаметром від 20 нм до 2–3 мкм. Зумовлена ними шорсткість поверхні змінюється в діапазоні від одиниць до кількох десятків нанометрів залежно від умов осадження шарів. Форма поверхневих утворень змінюється від гроноподібних дендритів фрактального типу до опуклих еліпсоїдів і багатокутників. Показано, що первинне структурування відбувається у вигляді утворення шару півсферичних мікрокрапель олова вже у процесі його осадження. Вторинне структурування відбувається на етапі осадження другого шару кремнію на шар олов'яних півсфер. На цьому етапі відбувається формування шару аморфного напівпровідника на поверхні рідинного металу, що досліджувалось вперше. Отриманий таким чином аморфний кремній має порувату структуру, що складається з гроно-подібних дендритів фрактального типу масштабу сотень нанометрів. Найменші елементи дендритів теж мають квазисферичну форму діаметром 20–50 нм. Отримані результати обговорені з точки зору можливих застосувань.

Ключові слова: аморфний кремній, олово, тонкі плівки, структура поверхні, нанокристали, термічне вакуумне напилення.